Pseudomonas aeruginosa High-Risk Sequence Type 463 Co-Producing KPC-2 and AFM-1 Carbapenemases, China, 2020–2022

Piaopiao Zhang,[1] Wenhao Wu,[1] Nanfei Wang, Haiting Feng, Jie Wang, Fang Wang, Yan Zhang, Hongchao Chen, Qing Yang, Yan Jiang,[2] Tingting Qu[2]

We report the clonal spread and evolution of high-risk *Pseudomonas aeruginosa* sequence type 463 co-producing KPC-2 and AFM-1 carbapenemases isolated from hospital patients in China during 2020–2022. Those strains pose a substantial public health threat and surveillance and stricter infection-control measures are essential to prevent further infections.

Carbapenemase-producing *Pseudomonas aeruginosa* poses a global threat to public health. Epidemics caused by this pathogen are associated with high-risk clones (e.g., sequence type [ST] 235, ST277, ST175, ST233 and ST111), particularly those clones producing metallo-β-lactamases; Verona integron-encoded metallo-β-lactamase and imipenemase are the most prevalent carbapenemase types (*1,2*). A *Klebsiella pneumoniae* carbapenemase (KPC)–producing clone, ST463, has emerged and become predominant in carbapenemase-producing *P. aeruginosa* populations in China (*3*). Three *P. aeruginosa* strains co-producing KPC and *Alcaligenes faecalis* metallo-β-lactamase (AFM) were reported in 2022 and attributed to ST463 (*4,5*). During 2020–2022, we observed the clonal spread of ST463 carbapenem-resistant *P. aeruginosa* (CRPA) co-producing KPC-2 and AFM-1

(KPC-2–AFM-1 CRPA) in a hospital in China, which caused infections with high mortality. We report on KPC-2–AFM-1 CRPA emergence and driving forces that caused dissemination.

The Study

During September 2020–June 2022, 192 nonduplicated CRPA isolates were collected from 192 patients admitted to a tertiary hospital in Zhejiang, China. Among those isolates, carbapenemase-producing *Pseudomonas aeruginosa* belonging to 10 different STs reached an overall prevalence of 41.1% (79/192) (Appendix Figure 1, https://wwwnc.cdc.gov/EID/article/29/10/23-0509-App1.pdf). We investigated KPC-2–AFM-1 CRPA strains isolated from 8 patients; 3 strains were colonizers and 5 were associated with infections (Table). The patients (6 men, 2 women) were 45–90 years of age, and all had complicated conditions and a history of intensive care unit admission. Antimicrobial drugs active against KPC-2–AFM-1 CRPA (colistin in monotherapy) were given to 4 patients; 5 infected patients eventually died; the remaining 3 patients, who only had bacterial colonization, were discharged (Table).

All 8 isolates were ST463, had identical resistance genes (Appendix Table 1) and type III secretion system genotype *exoU*+/*exoS*+, and differed by 5–30 single-nucleotide polymorphisms, indicating clonal dissemination (Appendix Figure 2). Each strain had 1 chromosome and a plasmid containing the β-lactamase gene *bla*KPC-2. Alignment of the 8 plasmids showed an identical backbone, but we noted major

Author affiliations: The First Affiliated Hospital of Zhejiang University School of Medicine, Hangzhou, China (P. Zhang, W. Wu, N. Wang, H. Feng, J. Wang, F. Wang, Y. Zhang, H. Chen, Q. Yang, T. Qu); Zhejiang University School of Medicine Sir Run Run Shaw Hospital, Hangzhou (Y. Jiang); Key Laboratory of Microbial Technology and Bioinformatics of Zhejiang Province, Hangzhou (Y. Jiang)

[1]These authors contributed equally to this article.

[2]These senior authors contributed equally to this article.

Table. Demographics and clinical characteristics of 8 patients infected by *Pseudomonas aeruginosa* high-risk sequence type 463 co-producing KPC-2 and AFM-1 carbapenemases, China, 2020–2022*

Patient no.	Strain	Age, y/sex	Ward	Underlying conditions	Sample isolation date	Sample type	Infection type	Therapy†	Outcome/Date
1	ZY94	90/M	ICU	Chronic kidney disease	2021 Feb 9	Sputum	Pulmonary infection	IMP, PTZ, COL	Death/2021 Feb 10
2	ZY156	77/M	ED	Acute toxic encephalopathy	2021 Feb 25	Urine	Urinary tract colonization	SCF	Discharge/2021 Mar 13
3	ZY1012	63/F	ICU	Intraabdominal malignancy	2021 Jul 26	Ascites	Intraabdominal infection	CZA, LEV, COL	Death/2021 Aug 20
4	ZY1075	79/M	ICU	Chronic cardiopulmonary disease	2021 Aug 12	Urine	Urinary tract colonization	NA	Discharge/2021 Aug 13
5	ZY1167	71/M	ICU	Hematologic malignancy	2021 Aug 28	Sputum	Pulmonary infection	IMP, PTZ, COL	Death/2021 Sep 13
6	ZY1214	45/M	Cardiac surgery	Aortic dissection	2021 Aug 31	Urine	Urinary tract colonization	SCF	Discharge/2021 Sep 8
7	ZY36	61/M	ICU	Chronic kidney disease	2022 Jan 9	Sputum	Pulmonary infection	IMP, SCF, COL	Death/2022 Jan 17
8	ZY1710	90/F	Geriatrics	Gallbladder carcinoma	2022 Apr 16	Sputum	Pulmonary infection	IMP	Death/2022 Apr 17

*AFM, *Alcaligenes faecalis* metallo-β-lactamase; COL, colistin; CZA, ceftazidime/avibactam; ED, emergency department; ICU, intensive care unit; IMP, imipenem; KPC, *Klebsiella pneumoniae* carbapenemase; LEV, levofloxacin, NA, not applicable (none); PTZ, piperacillin/tazobactam; SCF, cefperazone/sulbactam.
†Therapy began after bacterial isolation and identification.

differences within the insertion region; the conserved core bla_{KPC-2} genetic platform insertion sequence (IS) *Kpn27*–bla_{KPC-2}–IS*Kpn6* in plasmid p94 remained intact, whereas IS*Kpn6* and several genes immediately upstream (IS*Kpn6*–open reading frame–*klcA*–open reading frame) were absent in the other 7 plasmids (Appendix Figure 3, panel A), forming a novel genetic context for bla_{KPC-2}. All plasmids were designated as type I plasmids (*6*) but had a 16-kb deletion of a mobilization-related operon within the backbone (Appendix Figure 3, panel B), supporting their nontransferability, which was confirmed by conjugation assays.

Using phylogenetic analysis of 125 ST463 genomes (68 from the National Center for Biotechnology Information Reference Sequence database [https://www.ncbi.nlm.nih.gov/refseq] and 57 from our collection), we found that those genomes were divided into 2 clades (Figure 1). Collection dates for strains in clade 1 were much earlier than those for clade 2. Clade 1 was primarily represented by clones from the United States, and clade 1 isolates did not harbor bla_{KPC} or bla_{AFM}. The larger clade 2 originated in China and most isolates in this clade carried bla_{KPC}; we also detected bla_{AFM} in clade 2. Independent evolution of ST463 clones in China might be correlated with sequential acquisition of bla_{KPC} and bla_{AFM}. Paired single-nucleotide polymorphism distances for clade 2 strains in a minimum spanning tree were mainly 0–60 (Appendix Figure 2), demonstrating a high degree of relatedness among those isolates and clonal transmission of KPC-producing *P. aeruginosa* ST463 in China. The 8 KPC-2–AFM-1 CRPAs clustered with 3 bla_{AFM}-carrying strains and formed a separate subclade in-

side clade 2 that was surrounded by bla_{AFM}-negative, KPC-producing *P. aeruginosa*. Therefore, we inferred that ST463 KPC-2–AFM-1 CRPA clones probably arose from ST463 KPC-producing *P. aeruginosa*.

We could not map the genome sequences of clade 1 strains to the reference plasmid p94 (0% coverage), indicating the absence of type I plasmids in ST463 clones outside of China. Using BLAST (https://blast.ncbi.nlm.nih.gov), we retrieved 40 homologous plasmids that had >50% coverage and >95% identity to p94; all were type I plasmids carried by 14 different *P. aeruginosa* STs (Appendix Figure 4), suggesting an extensive horizontal transfer of type I plasmids within a narrow host range. Plasmid phylogeny revealed that all bla_{KPC-2}–encoding plasmids clustered together in an independent branch, and separation of that branch from closely related bla_{KPC-2}–negative plasmids might be associated with acquisition of bla_{KPC-2} (Appendix Figure 5). The presence of multiple copies of IS*26* in the bla_{KPC-2}–adjacent region beyond the core platform indicated a critical role for IS*26* elements in remodeling and resistance evolution of type I plasmids in the ST463 lineage (Appendix Figure 4) (*7*). We deduced an underlying evolutionary pathway: an ST463 *P. aeruginosa* progenitor initially acquired a highly transferable type I plasmid, which subsequently evolved into a resistance plasmid through IS*26*-mediated insertion events involving a bla_{KPC-2}–carrying region, then by chromosomal integration of bla_{AFM-1} to form KPC-2–AFM-1 CRPA. To further verify this hypothesis, we conducted a genomic comparison between ZY94 and the 1755 strain, which carried neither bla_{KPC} nor bla_{AFM} but was phylogenetically closest to the KPC-2–AFM-1

CRPA cluster (Figure 1). The genome of 1755 was also composed of 1 chromosome and 1 plasmid (p1755). Plasmid p94 was highly homologous (coverage 81%, identity 99.76%) to p1755 and might have evolved from p1755 via IS26-mediated intermolecular transposition of a bla_{KPC-2}–carrying translocatable unit that targeted an existing copy of IS26 (Appendix Figure 6, panel A). Comparisons between their chromosomes identified a redundant bla_{AFM-1}–containing, multidrug-resistance fragment bracketed by IS5564 in the same orientation, which was flanked by two 6-bp (GCTAGA) target site duplications (Appendix Figure 6, panel B), indicating a site-specific insertion event.

All 8 isolates were resistant to β-lactams and β-lactam/β-lactamase inhibitors, including carbapenems, ceftazidime/avibactam, fluoroquinolones, and gentamicin, and were only susceptible to amikacin and intermediately susceptible to colistin. We observed synergistic inhibitory effects against all 8 strains when we used combinations of ceftazidime/avibactam and aztreonam (Appendix Table 1). Compared with *P. aeruginosa* strain ATCC27853, all strains showed 4-fold higher MICs for chlorhexidine, a commonly used medical disinfectant, suggesting chlorhexidine tolerance (Appendix Table 1) (8).

All 8 strains exhibited small colony variant phenotypes together with strong biofilm formation capacities (Appendix Table 2). To assess their stability, desiccation resilience, and virulence, we selected strains ZY94 (infecting strain) and ZY1214 (colonizing strain) for further experiments. After we subcultured in antimicrobial drug–free Luria-Bertani broth for 10
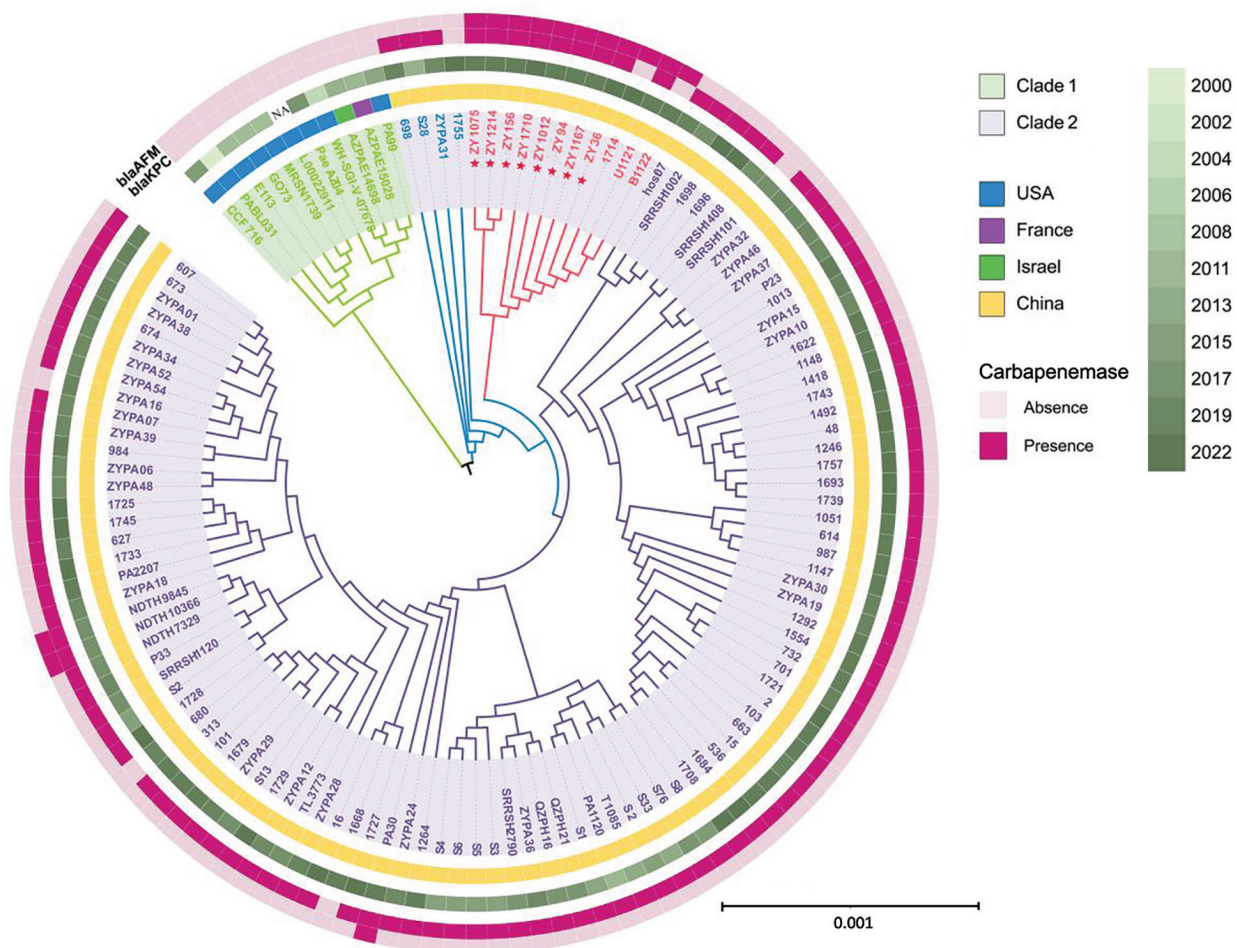

Figure 1. Phylogenetic analysis of *Pseudomonas aeruginosa* high-risk sequence type 463 strains co-producing KPC-2 and AFM-1 carbapenemases, China, 2020–2022. Core-genome phylogenetic tree was built for 125 *P. aeruginosa* sequence type 463 strains and rooted in the midpoint. Red asterisks indicate the 8 carbapenem-resistant *P. aeruginosa* strains co-producing KPC-2 and AFM-1 from a hospital in China. Presence and absence of bla_{AFM} and bla_{KPC} genes are indicated in the outermost 2 rings. Collection year, indicated by different shades of green, and location where each strain was isolated are indicated in the middle rings. The innermost shaded ring indicates strains belonging to clade 1 or 2. Scale bar indicates nucleotide substitutions per site. AFM, *Alcaligenes faecalis* metallo-β-lactamase; *bla*, β-lactamase; KPC, *Klebsiella pneumoniae* carbapenemase; NA, not available.
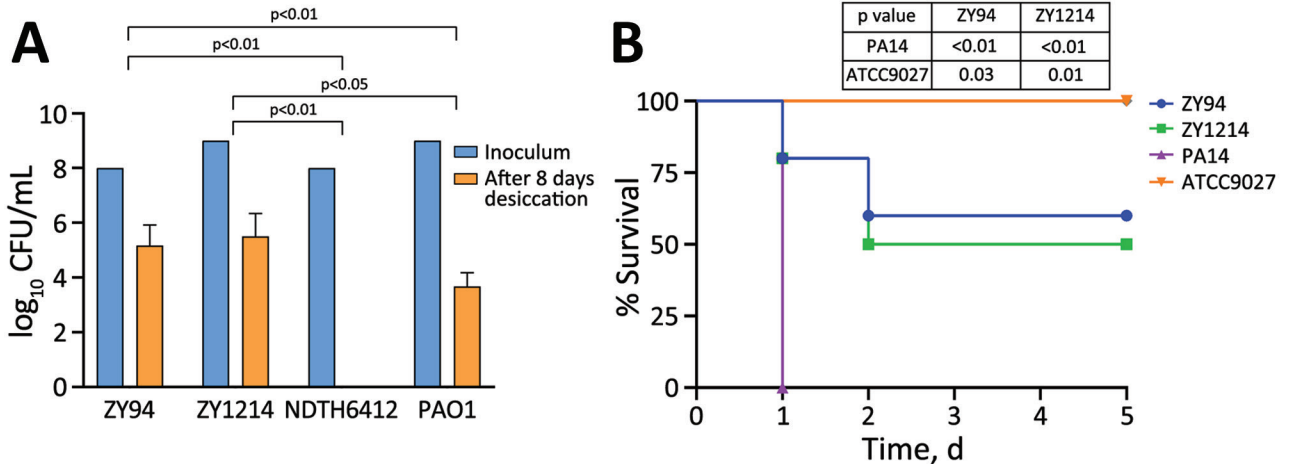
Figure 2. Desiccation tolerance and virulence analyses of *Pseudomonas aeruginosa* high-risk sequence type 463 co-producing KPC-2 and AFM-1 carbapenemases, China, 2020–2022. A) Carbapenem-resistant *P. aeruginosa* strains ZY94 and ZY1214 isolated from hospital patients in China were evaluated for desiccation tolerance. Results are given as mean (SD) CFU/mL for each isolate before and after 8 days of desiccation. Laboratory reference strain PAO1 and *P. aeruginosa* NDTH6412, which belongs to high-risk international sequence type 235, were used as controls. B) Virulence was determined by using Kaplan-Meier survival curves of mice intraperitoneally challenged with 1×10^7 CFUs of strain ZY94 or ZY1214, hypervirulent strain PA14, or nonvirulent *P. aeruginosa* strain ATCC9027. Mice (10 per group) were monitored for 5 days and the number of dead mice was assessed each day. Mantel-Cox log rank tests were used to calculate p values for survival curve comparisons between the different strains. AFM, *Alcaligenes faecalis* metallo-β-lactamase; CFUs, colony forming units; KPC, *Klebsiella pneumoniae* carbapenemase.

days, ZY94 and ZY1214 retained stable small colony variant phenotypes; their bla_{KPC-2}–carrying plasmid and bla_{AFM-1} gene were both stably inherited (stability was 93% for ZY94 and 95% for ZY1214). Both strains survived for 8 days on a dry polystyrene surface at higher rates than strains PAO1 and NDTH6412 (Figure 2, panel A). Furthermore, in mouse intraperitoneal challenge models (Appendix), ZY94 and ZY1214 strains had significantly higher (≈50%) lethality than ATCC9027 (p<0.05), but were less virulent than the PA14 strain (Figure 2, panel B).

Conclusions

We documented the persistent clonal spread of ST463 KPC-2–AFM-1 CRPAs in a hospital in China and provided insights into a potential evolutionary pathway for KPC-2–AFM-1 CRPA formation. Extensive drug resistance, disinfectant and desiccation resilience, strong biofilm formation, and high stability constituted strategies for those strains to defend against host and clinical challenges, thereby driving persistent transmission of this high-risk clone. Infections caused by such pathogens might lead to high death rates, especially in immunocompromised or critically ill patients, highlighting the urgent need for effective infection prevention and control policies. ST463 KPC-2–AFM-1 CRPA strains pose a substantial public health threat because of their extensive drug resistance, considerable pathogenicity,

and ability to persist in the environment. Targeted surveillance and stricter infection-control measures are essential to prevent further infection outbreaks.

This study was approved by the institutional review board of the First Affiliated Hospital of Zhejiang University School of Medicine in China (approval no. IIT20210120B).

About the Author

Dr. Zhang is a resident doctor at the First Affiliated Hospital of Zhejiang University School of Medicine, in Hangzhou, Zhejiang, China. Her primary research interests are antimicrobial drug resistance and *Pseudomonas aeruginosa* epidemiology.

References

1. Del Barrio-Tofiño E, López-Causapé C, Oliver A. *Pseudomonas aeruginosa* epidemic high-risk clones and their association with horizontally-acquired β-lactamases: 2020 update. Int J Antimicrob Agents. 2020;56:106196. https://doi.org/10.1016/j.ijantimicag.2020.106196
2. Reyes J, Komarow L, Chen L, Ge L, Hanson BM, Cober E, et al.; Antibacterial Resistance Leadership Group and Multi-Drug Resistant Organism Network Investigators. Global epidemiology and clinical outcomes of
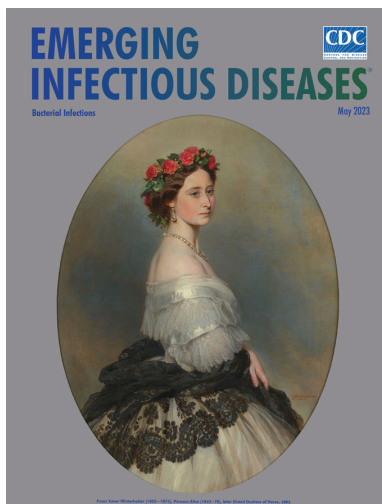
carbapenem-resistant *Pseudomonas aeruginosa* and associated carbapenemases (POP): a prospective cohort study. Lancet Microbe. 2023;4:e159–70. https://doi.org/10.1016/S2666-5247(22)00329-9

3. Hu Y, Liu C, Wang Q, Zeng Y, Sun Q, Shu L, et al. Emergence and expansion of a carbapenem-resistant *Pseudomonas aeruginosa* clone are associated with plasmid-borne *bla*_{KPC-2} and virulence-related genes. mSystems. 2021; 6:e00154-21. https://doi.org/10.1128/mSystems.00154-21

4. Li Y, Zhu Y, Zhou W, Chen Z, Moran RA, Ke H, et al. *Alcaligenes faecalis* metallo-β-lactamase in extensively drug-resistant *Pseudomonas aeruginosa* isolates. Clin Microbiol Infect. 2022;28:880.e1–8. PubMed https://doi.org/10.1016/j.cmi.2021.11.012

5. Zhang P, Wang J, Shi W, Wang N, Jiang Y, Chen H, et al. In vivo acquisition of bla_{KPC-2} with low biological cost in bla_{AFM-1}–harboring ST463 hypervirulent *Pseudomonas aeruginosa* from a patient with hematologic malignancy. J Glob Antimicrob Resist. 2022;31:189–95. https://doi.org/10.1016/j.jgar.2022.09.004

6. Zhu Y, Chen J, Shen H, Chen Z, Yang QW, Zhu J, et al. Emergence of ceftazidime- and avibactam-resistant *Klebsiella pneumoniae* carbapenemase-producing *Pseudomonas aeruginosa* in China. mSystems. 2021;6:e0078721. https://doi.org/10.1128/mSystems.00787-21

7. He S, Hickman AB, Varani AM, Siguier P, Chandler M, Dekker JP, et al. Insertion sequence IS*26* reorganizes plasmids in clinically isolated multidrug-resistant bacteria by replicative transposition. mBio. 2015;6:e00762. https://doi.org/10.1128/mBio.00762-15

8. Sahin S, Mogulkoc MN, Kürekci C. Disinfectant and heavy metal resistance profiles in extended spectrum β-lactamase (ESBL) producing *Escherichia coli* isolates from chicken meat samples. Int J Food Microbiol. 2022;377:109831. https://doi.org/10.1016/j.ijfoodmicro.2022.109831

Address for correspondence: Tingting Qu, The First Affiliated Hospital of Zhejiang University School of Medicine, No.79 Qingchun Rd, Hangzhou 310000, China; email: qutingting@zju.edu.cn

May 2023
Bacterial Infections

EMERGING INFECTIOUS DISEASES®

To revisit the May 2023 issue, go to:
https://wwwnc.cdc.gov/eid/articles/issue/29/5/table-of-contents

Pseudomonas aeruginosa High-Risk Sequence Type 463 Co-Producing KPC-2 and AFM-1 Carbapenemases, China, 2020–2022

Appendix

Detailed Methods

Bacterial Isolation and Clinical Data Collection

During September 2020–June 2022, a total of 192 nonduplicated clinical carbapenem-resistant *Pseudomonas aeruginosa* (CRPA) isolates were collected from patients in a tertiary hospital in Zhejiang, China, and were subjected to whole-genome sequencing for further molecular investigation. Eight CRPA strains co-producing *Klebsiella pneumoniae* carbapenemase (KPC) and *Alcaligenes faecalis* metallo-β-lactamase (AFM) (KPC-2–AFM-1 CRPA strains) were identified. Demographics and relevant clinical data were obtained through review of medical records. An infected case-patient was defined according to the US Centers for Disease Control and Prevention criteria (*1*); a colonized case-patient was defined as a patient carrying CRPA without clinical evidence of infection.

Antimicrobial Susceptibility Testing

MICs for 13 routine antimicrobial agents used to treat *P. aeruginosa* and chlorhexidine, a commonly used medical disinfectant, were determined by using the broth microdilution method. Clinical breakpoints of all antimicrobial drugs were interpreted according to the 2021 Clinical and Laboratory Standards Institute guidelines (*2*); *P. aeruginosa* ATCC27853 and *K. pneumoniae* ATCC700603 served as quality control strains. Accepted interpretive criteria have not been defined for disinfectants according to MIC values; therefore, comparing obtained results with those of the reference strain ATCC27853 might prove valuable.

Checkerboard Susceptibility Assay

In vitro synergistic inhibitory activities of ceftazidime/avibactam and aztreonam against all 8 isolates were determined in duplicate by using the broth microdilution checkerboard assay as previously described (*3*). The concentrations tested ranged from $\leq 1/32 \times$ MIC to $2 \times$ MIC for each antimicrobial drug. The interactions between antimicrobial agents were determined by calculating the fractional inhibitory concentration index (FICI). FICIs were interpreted as follows: FICI ≤ 0.5 = synergy, FICI >0.5 to ≤ 1 = additive, FICI >1 to ≤ 4 = no interaction, and FICI >4 = antagonism.

Whole-Genome Sequencing and Bioinformatics Analysis

Genomic DNA from 192 isolates was extracted and then sequenced by using the Illumina HiSeq X Ten platform (Illumina, https://www.illumina.com). Clean reads generated by Illumina sequencing were de novo assembled by using Shovill version 0.9.0 (https://github.com/tseemann/shovill). Long reads were sequenced for 8 KPC-2–AFM-1 CRPA isolates by using a MinION sequencer device (Oxford Nanopore Technologies, https:/www.nanoporetech.com). Hybrid assemblies of Illumina short reads and MinION long reads were prepared with Unicycler version 0.4.8 (*4*). Multilocus sequence typing was performed by using an mlst tool (https://github.com/tseemann/mlst). Antimicrobial drug resistance and virulence genes were identified with ABRicate version 1.0.0 (https://github.com/tseemann/abricate) according to the National Center for Biotechnology Information (NCBI) AMRFinderPlus (https://www.ncbi.nlm.nih.gov) and virulence factor (http://www.mgc.ac.cn/VFs) databases. Pairwise single-nucleotide polymorphism (SNP) distance was evaluated with Snp-dists (https://github.com/tseemann/snp-dists). Sequence comparisons were performed by using Easyfig version 2.2.3 and annotated by BacAnt and Prokka (*5,6*). Alignments and visualization of plasmids were generated by BLAST Ring Image Generator (BRIG) software version 0.95 (https://sourceforge.net/projects/brig).

Phylogenetic Analysis

A phylogenetic tree for all ST463 *P. aeruginosa* genomes from the NCBI database and our collection was constructed according to their SNPs by using Snippy version 4.4.5 (https://github.com/tseemann/snippy) and FastTree (*7*). The genome of strain B1122 (GenBank accession no. JAMWMN000000000) was used as a reference. As of September 2022, a total of 6,885 *P. aeruginosa* assembled genomes had been deposited in the NCBI Reference Sequence

database (https://www.ncbi.nlm.nih.gov/refseq), among which 68 genomes were assigned to ST463 and were downloaded for phylogenetic analysis.

The maximum likelihood phylogenetic tree for p94-related plasmid sequences was inferred from a core genome alignment by using Panaroo version 1.2.7 (*8*) and IQ-TREE version 2.1.2 (*9*). All trees were visualized in iTOL (https://itol.embl.de).

Plasmid Conjugation

The transferability of plasmids p94 and p1214 was evaluated by conjugation experiments; the filter mating method was used with a rifampin-resistant derivative of *P. aeruginosa*, PAO1, as the recipient strain. Transconjugants were selected on Mueller-Hinton agar plates supplemented with rifampin (800 μg/mL) and meropenem (4 μg/mL). Experiments were independently repeated 3 times.

Stability of bla_{KPC-2}–Carrying Plasmid and Chromosome-Encoded bla_{AFM-1}

To determine the stability of the bla_{KPC-2}–carrying plasmid and chromosomal bla_{AFM-1} gene, a passaging experiment was completed under antibiotic-free conditions. Briefly, 3 separate bacterial cultures were prepared by inoculating 3 mL Luria-Bertani (LB) broth without antibiotics and incubating overnight at 37°C, then a serial passage of 3 μL overnight culture into 3 mL LB was prepared each day. Samples were collected and diluted on Mueller-Hinton agar plates on day 10. Then, 48 colonies were randomly selected for validation of the presence of bla_{KPC-2}, *repA*, and bla_{AFM-1} by PCR with gene-specific primers. Retention was calculated as the percentage of cells with bla_{KPC-2}, *repA*, and bla_{AFM-1} in the 48 selected colonies.

Biofilm Quantification and Desiccation Tolerance

Biofilm quantification was performed by using crystal violet staining as described previously (*10*). Biofilm formation capabilities were assessed according to a published study (*11*). The capacity to survive on dry surfaces over time was evaluated as described previously with some minor modifications (*12*). Briefly, 100 μL of an overnight bacteria culture was serially diluted and counted the next day. Another 100 μL of the same culture was transferred into a 96-well microtiter plate; 3 technical replicates were prepared. The plate was air dried overnight and then incubated at 37°C for 8 days. Subsequently, 100 μL/well of fresh LB broth was added to the plate, and the plate was incubated with shaking at 37°C for 3 h. From each well, 100 μL of

suspension was collected, serially diluted, and counted the next day. Experiments were conducted in triplicate.

Mouse Peritonitis Model

Male immunocompetent BALB/c mice (6–8 weeks of age, weighing 20–25 g) were injected intraperitoneally with 100 μL phosphate-buffered saline solution containing 1×10^7 CFU of a *P. aeruginosa* strain in exponential growth phase (10 mice/group). PA14 was used as a hypervirulent reference strain, and *P. aeruginosa* ATCC9027 was a low-virulence reference strain (*13*). After inoculation, mice were monitored for 5 days, and the number of dead mice was assessed each day. All animal experiments were approved by the Institutional Animal Care and Ethics Committee of the First Affiliated Hospital of Zhejiang University School of Medicine.

Statistics

Statistical analysis was performed by using GraphPad Prism software, version 9.0 (GraphPad, https://www.graphpad.com). The Mann-Whitney U-test was applied for pairwise comparison of bacterial groups by using mean values. Survival curves for the mouse infection model were analyzed by log-rank (Mantel-Cox) test. p values of <0.05 were statistically significant.

Data Availability

The sequencing data for 8 isolates from this study have been deposited in GenBank under accession nos. JARDUM000000000, JARDUN000000000, JARDUO000000000, JARDUP000000000, CP125361-CP125362, CP125363-CP125364, CP125365-CP125366, and CP125367-CP125368.

References

1. Garner JS, Jarvis WR, Emori TG, Horan TC, Hughes JM. CDC definitions for nosocomial infections, 1988. Am J Infect Control. 1988;16:128–40. PubMed https://doi.org/10.1016/0196-6553(88)90053-3

2. Clinical and Laboratory Standards Institute. Performance standards for antimicrobial susceptibility testing; thirty-first edition (M100-Ed31). Wayne (PA): The Institute; 2021.

3. Al-Quraini M, Rizvi M, Al-Jabri Z, Sami H, Al-Muzahmi M, Al-Muharrmi Z, et al. Assessment of in-vitro synergy of fosfomycin with meropenem, amikacin and tigecycline in whole genome

sequenced extended and pan drug resistant *Klebsiella pneumoniae*: exploring a colistin sparing protocol. Antibiotics (Basel). 2022;11:153. PubMed https://doi.org/10.3390/antibiotics11020153

4. Wick RR, Judd LM, Gorrie CL, Holt KE. Unicycler: resolving bacterial genome assemblies from short and long sequencing reads. PLOS Comput Biol. 2017;13:e1005595. PubMed https://doi.org/10.1371/journal.pcbi.1005595

5. Hua X, Liang Q, Deng M, He J, Wang M, Hong W, et al. BacAnt: a combination annotation server for bacterial DNA sequences to identify antibiotic resistance genes, integrons, and transposable elements. Front Microbiol. 2021;12:649969. PubMed https://doi.org/10.3389/fmicb.2021.649969

6. Seemann T. Prokka: rapid prokaryotic genome annotation. Bioinformatics. 2014;30:2068–9. PubMed https://doi.org/10.1093/bioinformatics/btu153

7. Price MN, Dehal PS, Arkin AP. FastTree 2—approximately maximum-likelihood trees for large alignments. PLoS One. 2010;5:e9490. PubMed https://doi.org/10.1371/journal.pone.0009490

8. Tonkin-Hill G, MacAlasdair N, Ruis C, Weimann A, Horesh G, Lees JA, et al. Producing polished prokaryotic pangenomes with the Panaroo pipeline. Genome Biol. 2020;21:180. PubMed https://doi.org/10.1186/s13059-020-02090-4

9. Nguyen LT, Schmidt HA, von Haeseler A, Minh BQ. IQ-TREE: a fast and effective stochastic algorithm for estimating maximum-likelihood phylogenies. Mol Biol Evol. 2015;32:268–74. PubMed https://doi.org/10.1093/molbev/msu300

10. Zhang P, Wang J, Shi W, Wang N, Jiang Y, Chen H, et al. In vivo acquisition of bla_{KPC-2} with low biological cost in bla_{AFM-1}–harboring ST463 hypervirulent *Pseudomonas aeruginosa* from a patient with hematologic malignancy. J Glob Antimicrob Resist. 2022;31:189–95. PubMed https://doi.org/10.1016/j.jgar.2022.09.004

11. Macias-Valcayo A, Aguilera-Correa JJ, Broncano A, Parron R, Auñon A, Garcia-Cañete J, et al. Comparative in vitro study of biofilm formation and antimicrobial susceptibility in gram-negative bacilli isolated from prosthetic joint infections. Microbiol Spectr. 2022;10:e0085122. PubMed https://doi.org/10.1128/spectrum.00851-22

12. Heiden SE, Hübner NO, Bohnert JA, Heidecke CD, Kramer A, Balau V, et al. A *Klebsiella pneumoniae* ST307 outbreak clone from Germany demonstrates features of extensive drug resistance, hypermucoviscosity, and enhanced iron acquisition. Genome Med. 2020;12:113. PubMed https://doi.org/10.1186/s13073-020-00814-6

13. Grosso-Becerra MV, González-Valdez A, Granados-Martínez MJ, Morales E, Servín-González L, Méndez JL, et al. *Pseudomonas aeruginosa* ATCC 9027 is a non-virulent strain suitable for mono-rhamnolipids production. Appl Microbiol Biotechnol. 2016;100:9995–10004. PubMed https://doi.org/10.1007/s00253-016-7789-9

Appendix Table 1. Antimicrobial drug susceptibility profiles and resistance genes for the 8 ST463 KPC-2–AFM-1–CRPA isolates from China*

| Strain	MEM	IMP	CAZ	FEP	PIP	AZT	AK	GEN	LEV	CIP	P/T	CZA	COL	CHG	FICI CZA/AZT	Molecule	Antimicrobial resistance genes
ZY94	>128	>128	>128	>128	>128	>128	4	128	128	8	>128/4	>128/4	2	16	0.08	Chromosome	*aac(6')-Ib-G*, *aph(3'')-Ib*, *aph(3')-IIb*, *aph(6)-Id*, *bla*_{AFM-1}, *bla*_{CARB-2}, *bla*_{OXA-486}, *catB7*, *bla*_{PDC-374}, *ble*_{MBL}, *cmx* (×2), *crpP*, *floR2*, *fosA*, *mph(E)*, *msr(E)*, *sul1* (×2), *tet(G)*
																Plasmid	*bla*_{KPC-2}
ZY156	>128	>128	>128	>128	>128	>128	1	128	64	8	>128/4	>128/4	1	16	0.08	Chromosome	*aac(6')-Ib-G*, *aph(3'')-Ib*, *aph(3')-IIb*, *aph(6)-Id*, *bla*_{AFM-1}, *bla*_{CARB-2}, *bla*_{OXA-486}, *catB7*, *bla*_{PDC-374}, *ble*_{MBL}, *cmx* (×2), *crpP*, *floR2*, *fosA*, *mph(E)*, *msr(E)*, *sul1* (×2), *tet(G)*
																Plasmid	*bla*_{KPC-2}
ZY1012	>128	>128	>128	>128	>128	>128	4	128	64	16	>128/4	>128/4	2	16	0.08	Chromosome	*aac(6')-Ib-G*, *aph(3'')-Ib*, *aph(3')-IIb*, *aph(6)-Id*, *bla*_{AFM-1}, *bla*_{CARB-2}, *bla*_{OXA-486}, *catB7*, *bla*_{PDC-374}, *ble*_{MBL}, *cmx* (×2), *crpP*, *floR2*, *fosA*, *mph(E)*, *msr(E)*, *sul1* (×2), *tet(G)*
																Plasmid	*bla*_{KPC-2}
ZY1075	>128	>128	>128	>128	>128	>128	8	128	64	16	>128/4	>128/4	2	16	0.08	Chromosome	*aac(6')-Ib-G*, *aph(3'')-Ib*, *aph(3')-IIb*, *aph(6)-Id*, *bla*_{AFM-1}, *bla*_{CARB-2}, *bla*_{OXA-486}, *catB7*, *bla*_{PDC-374}, *ble*_{MBL}, *cmx* (×2), *crpP*, *floR2*, *fosA*, *mph(E)*, *msr(E)*, *sul1* (×2), *tet(G)*
																Plasmid	*bla*_{KPC-2}
ZY1167	>128	>128	>128	>128	>128	>128	4	128	64	16	>128/4	>128/4	1	16	0.16	Chromosome	*aac(6')-Ib-G*, *aph(3'')-Ib*, *aph(3')-IIb*, *aph(6)-Id*, *bla*_{AFM-1}, *bla*_{CARB-2}, *bla*_{OXA-486}, *catB7*, *bla*_{PDC-374}, *ble*_{MBL}, *cmx* (×2), *crpP*, *floR2*, *fosA*, *mph(E)*, *msr(E)*, *sul1* (×2), *tet(G)*
																Plasmid	*bla*_{KPC-2}
ZY1214	>128	>128	>128	>128	>128	>128	8	128	64	16	>128/4	>128/4	1	16	0.16	Chromosome	*aac(6')-Ib-G*, *aph(3'')-Ib*, *aph(3')-IIb*, *aph(6)-Id*, *bla*_{AFM-1}, *bla*_{CARB-2}, *bla*_{OXA-486}, *catB7*, *bla*_{PDC-374}, *ble*_{MBL}, *cmx* (×2), *crpP*, *floR2*, *fosA*, *mph(E)*, *msr(E)*, *sul1* (×2), *tet(G)*
																Plasmid	*bla*_{KPC-2}
ZY36	>128	>128	>128	>128	>128	>128	8	128	64	16	>128/4	>128/4	1	16	0.14	Chromosome	*aac(6')-Ib-G*, *aph(3'')-Ib*, *aph(3')-IIb*, *aph(6)-Id*, *bla*_{AFM-1}, *bla*_{CARB-2}, *bla*_{OXA-486}, *catB7*, *bla*_{PDC-374}, *ble*_{MBL}, *cmx* (×2), *crpP*, *floR2*, *fosA*, *mph(E)*, *msr(E)*, *sul1* (×2), *tet(G)*
																Plasmid	*bla*_{KPC-2}
ZY1710	>128	>128	>128	>128	>128	>128	8	128	64	16	>128/4	>128/4	1	16	0.27	Chromosome	*aac(6')-Ib-G*, *aph(3'')-Ib*, *aph(3')-IIb*, *aph(6)-Id*, *bla*_{AFM-1}, *bla*_{CARB-2}, *bla*_{OXA-486}, *catB7*, *bla*_{PDC-374}, *ble*_{MBL}, *cmx* (×2), *crpP*, *floR2*, *fosA*, *mph(E)*, *msr(E)*, *sul1* (×2), *tet(G)*
																Plasmid	*bla*_{KPC-2}
ATCC 27853	0.5	2	2	1	2	4	2	1	1	0.5	4/4	NA	0.5	4	NA	NA	NA

*AFM, *Alcaligenes faecalis* metallo-β-lactamase; AK, amikacin; ATCC, American Type Culture Collection (https://www.atcc.org); AZT, aztreonam; CAZ, ceftazidime; CHG, chlorhexidine; CIP, ciprofloxacin; COL, colistin; CRPA, carbapenem-resistant *Pseudomonas aeruginosa*; CZA, ceftazidime/avibactam; FEP, cefepime; FICI, fractional inhibitory concentration index; GEN, gentamicin; IPM, imipenem; KPC, *Klebsiella pneumoniae* carbapenemase; LEV, levofloxacin; MEM, meropenem; NA, not applicable; PIP, piperacillin; P/T, piperacillin/tazobactam; ST463, sequence type 463.

Appendix Table 2. Quantitative data for biofilm formation by 8 KPC-2–AFM-1 CRPA isolates from China*

Strain	Optical density at 590 nm								
ZY36	1.128	0.835	1.445	1.142	1.129	1.416	1.13	1.379	1.575
ZY94	1.039	0.897	0.921	0.73	1.023	1.072	0.811	0.866	1.402
ZY156	0.972	0.816	0.771	0.867	0.83	0.811	0.865	0.834	1.293
ZY1012	0.782	0.782	0.855	0.85	0.892	0.81	0.986	0.896	1.031
ZY1075	1.029	0.854	1.167	1.052	1.051	1.077	1.098	0.889	1.557
ZY1167	0.981	1.14	1.329	0.954	1.117	1.259	1.203	1.004	1
ZY1214	0.877	0.951	0.947	0.879	0.829	0.895	0.829	0.937	1.116
ZY1710	1.012	0.958	0.988	0.803	0.814	0.939	0.933	0.93	1.176
Negative control	0.113	0.119	0.133	0.111	0.144	0.115	0.124	0.123	0.113

*AFM, *Alcaligenes faecalis* metallo-β-lactamase; CRPA, carbapenem-resistant *Pseudomonas aeruginosa*; KPC, *Klebsiella pneumoniae* carbapenemase.
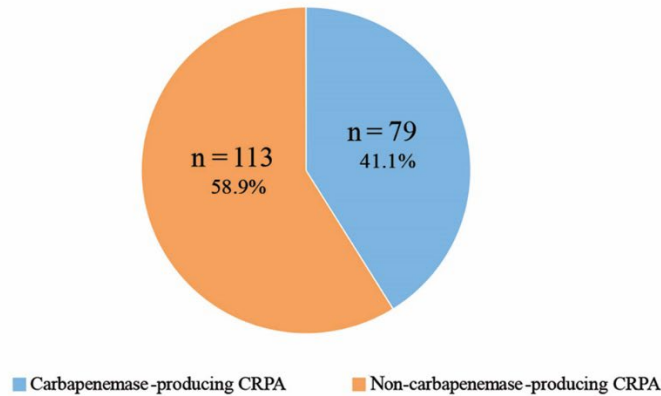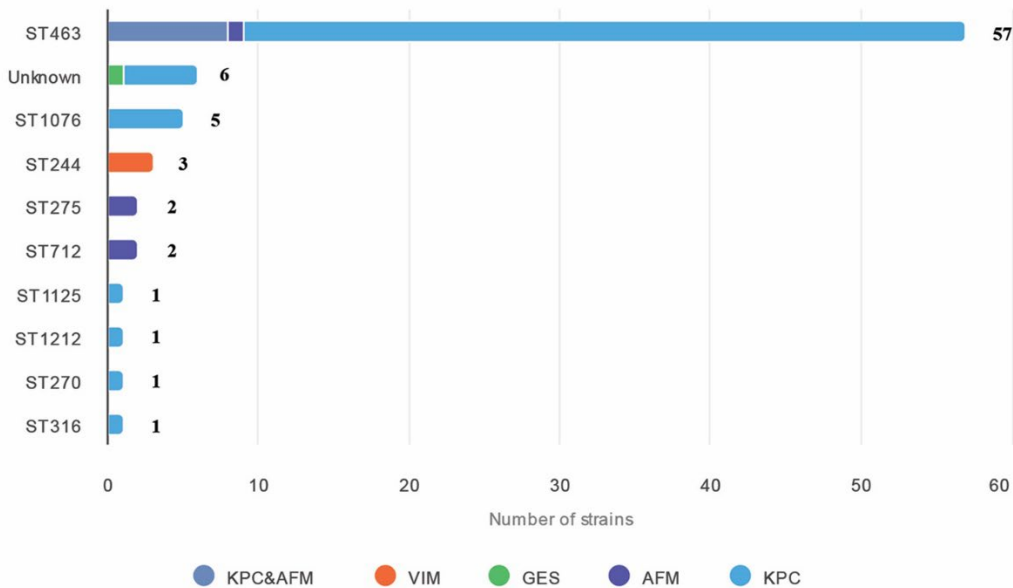

Appendix Figure 1. Distribution of carbapenem-resistant *Pseudomonas aeruginosa* strains isolated from hospital patients in Zhejiang, China during 2020–2022. A) Prevalence of carbapenemase-producing and noncarbapenemase-producing strains. B) Number and distribution of carbapenemases in 10

carbapenemase-producing *P. aeruginosa* sequence types. AFM, *Alcaligenes faecalis* metallo-β-lactamase; CRPA, carbapenem-resistant *P. aeruginosa*; GES, Guiana extended-spectrum β-lactamase; KPC, *Klebsiella pneumoniae* carbapenemase; ST, sequence type; VIM, Verona integron-encoded metallo-β-lactamase.
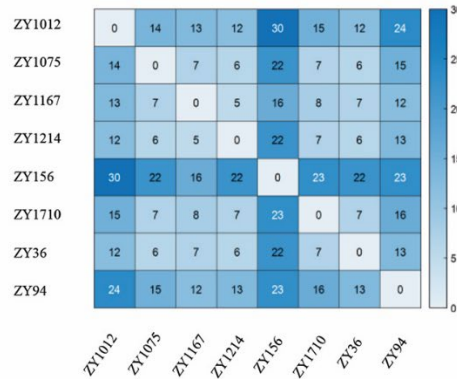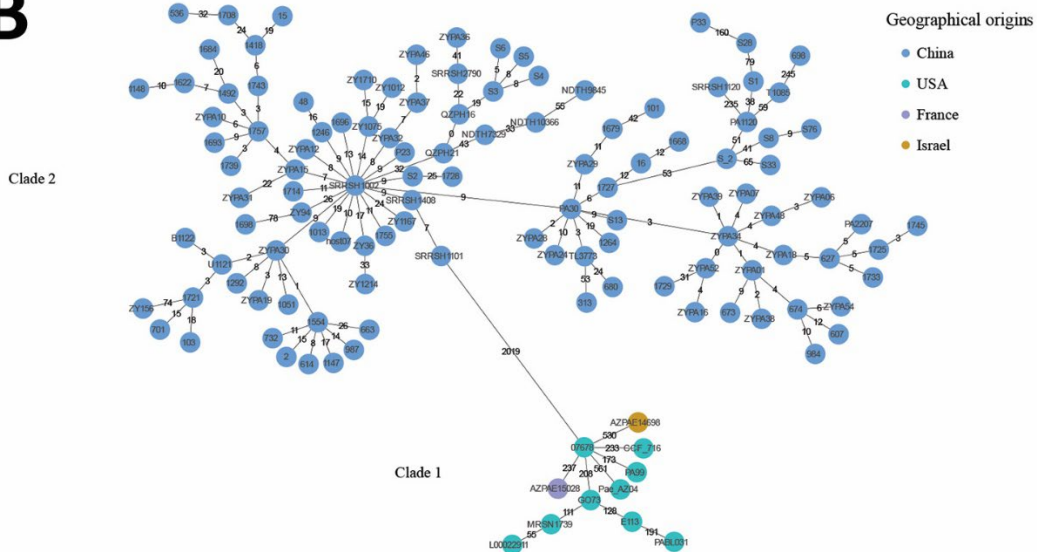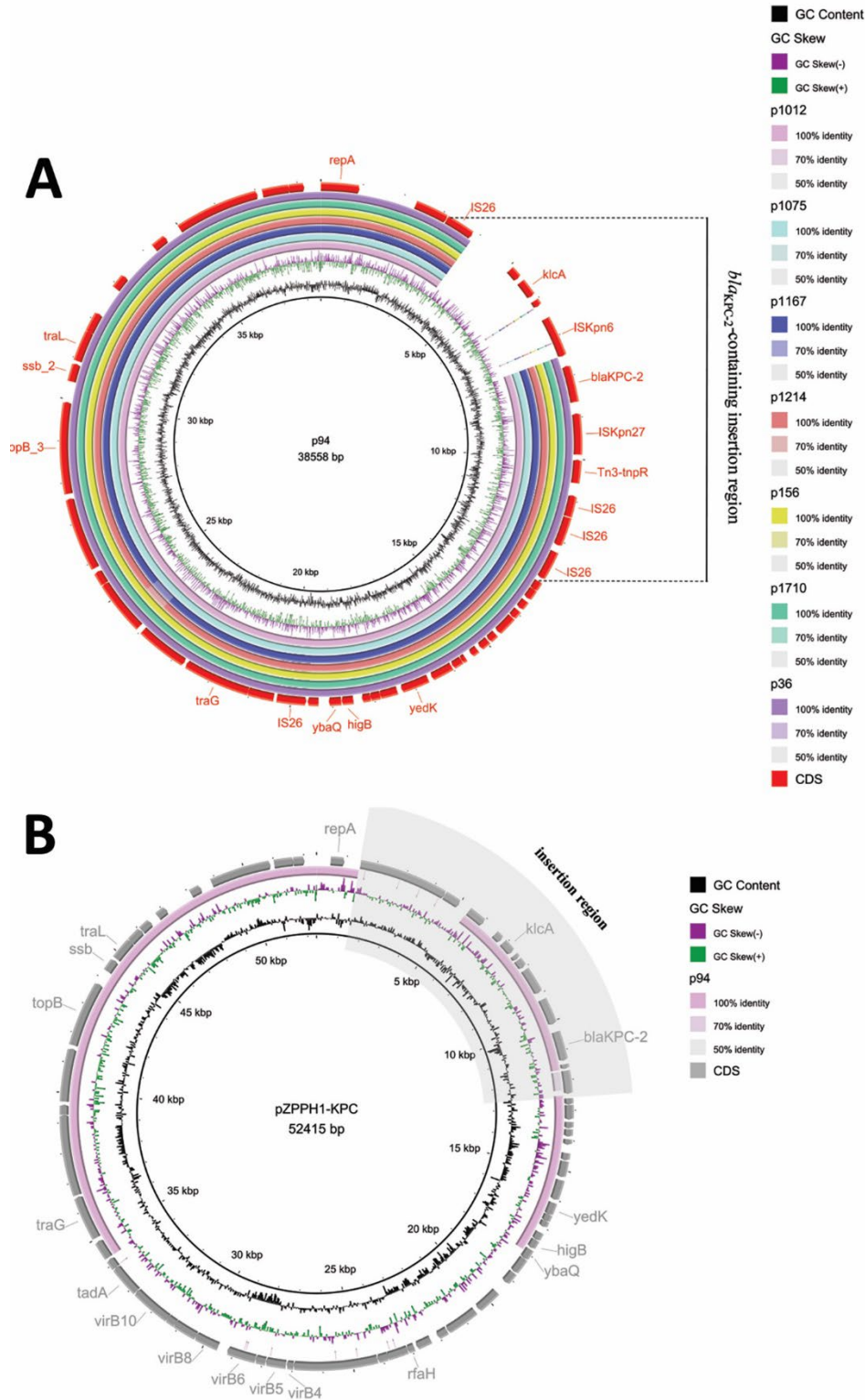

Appendix Figure 2. Single-nucleotide polymorphism distances and minimum spanning tree analysis of sequence type 463 carbapenem-resistant *Pseudomonas aeruginosa* strains isolated during this study that co-produced *Klebsiella pneumoniae* carbapenemase-2 and *Alcaligenes faecalis* metallo-β-lactamase-1. A) Paired single-nucleotide polymorphism (SNP) distances between each strain. B) Minimum spanning tree of 125 sequence type 463 isolates according to core SNPs. Each circle indicates an individual strain; different fill colors indicate geographic origin of each strain. Numbers on connecting lines indicate the number of SNPs in a pairwise comparison.

Appendix Figure 3. Alignments and genetic organization of plasmids from sequence type 463 carbapenem-resistant *Pseudomonas aeruginosa* strains isolated during this study that co-produced *Klebsiella pneumoniae* carbapenemase-2 and *Alcaligenes faecalis* metallo-β-lactamase-1. A) Alignment

of complete *bla*KPC-2-containing plasmids from 8 carbapenem-resistant *P. aeruginosa* isolates obtained in this study. Plasmid p94 from strain ZY94 is the reference sequence. B) Genetic organization of archetypal type I plasmid pZPPH1-KPC (GenBank accession no. CP077990) and comparison with p94 isolated in this study. Structure of pZPPH1-KPC consists of backbone and insertion regions (shaded gray). Outermost ring is an annotation of the reference plasmids (p94 and pZPPH1-KPC) and shows the direction of the transcriptional open reading frame. GC-rich regions (GC skew) are indicated. CDS, coding sequence.
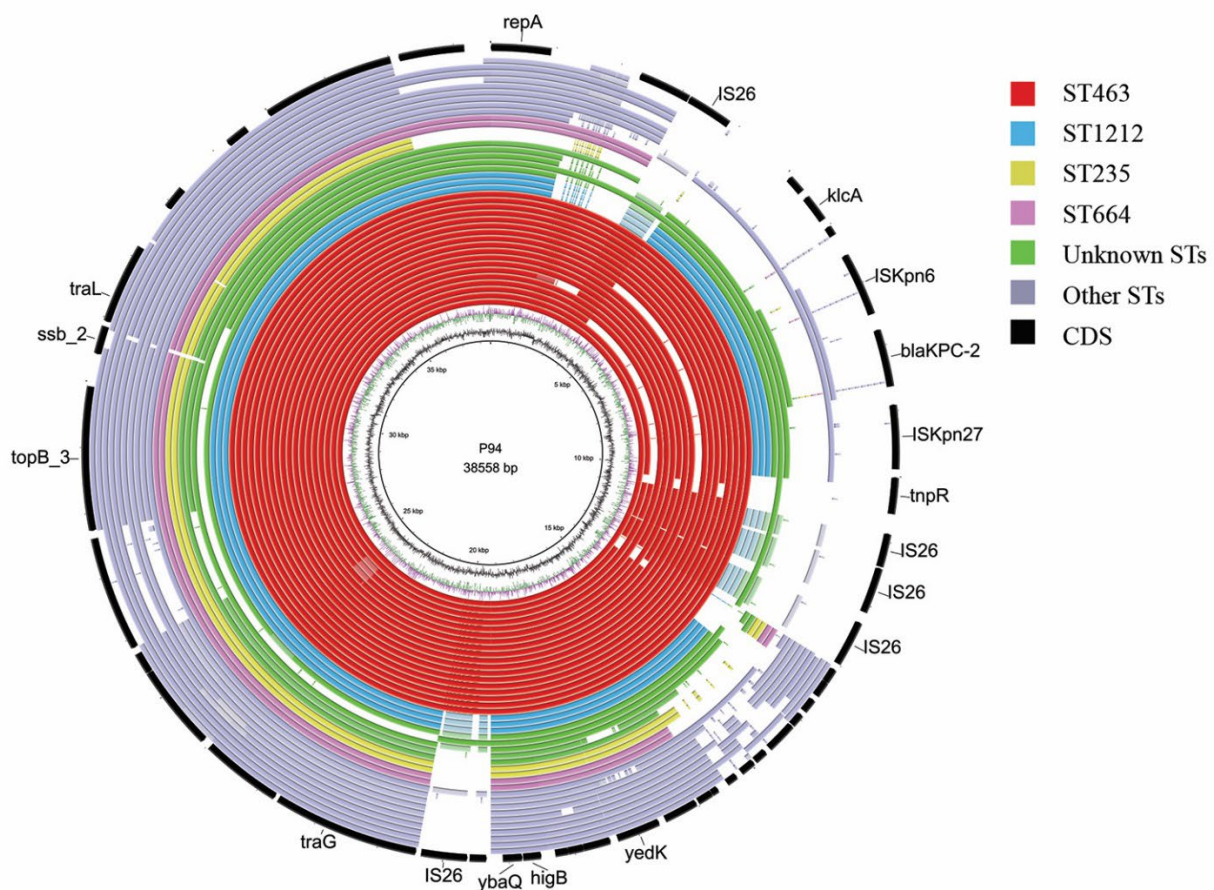
Appendix Figure 4. Comparison of plasmid p94 from this study and homologous plasmids isolated from other *Pseudomonas aeruginosa* strains. BLAST Ring Image Generator (https://sourceforge.net/projects/brig) diagram shows p94 in the innermost ring and alignments with 40 related plasmids. Colored rings indicate different *P. aeruginosa* sequence types. The outermost black ring shows genes on p94. CDS, coding sequence; ST, sequence type.
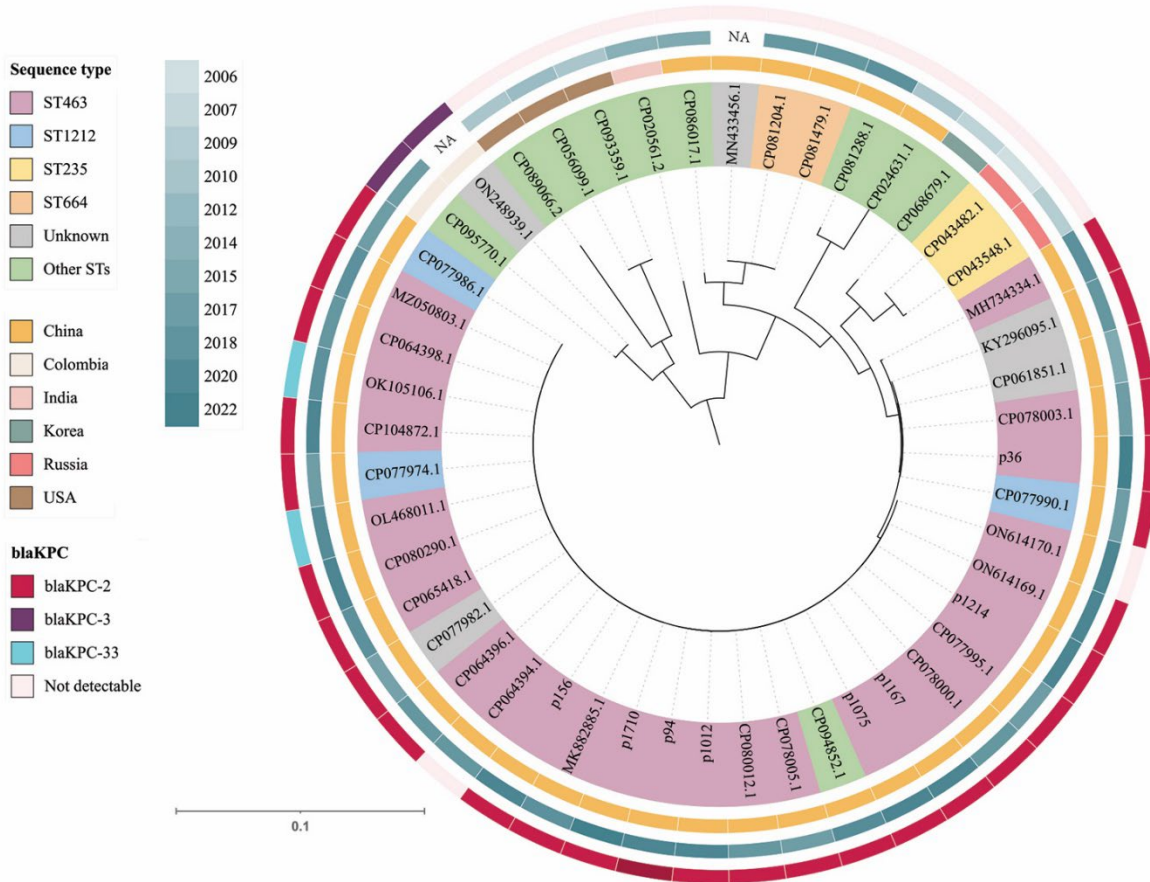
Appendix Figure 5. Phylogenetic analysis of 8 p94-related plasmids from this study and 40 related plasmids from GenBank. The outermost ring indicates the presence of different *Klebsiella pneumoniae* carbapenemase genes. The 2 middle rings indicate the isolate collection year and origin. GenBank accession nos. are indicated. Scale bar indicates nucleotide substitutions per site. NA, not available; ST, sequence type.
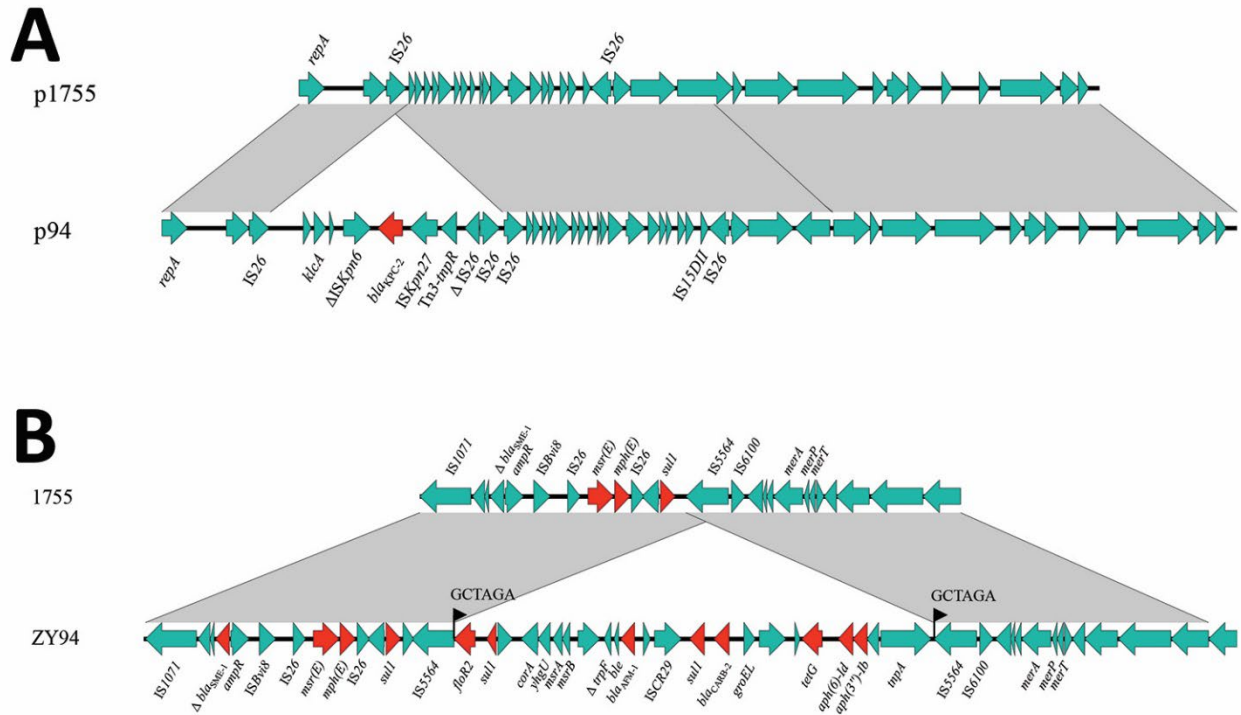
Appendix Figure 6. Genomic comparison of plasmid and chromosome sequences between strains ZY94 from this study and 1755. A) Co-linear genome alignment of plasmids p1755 and p94. B) Comparison of partial chromosomes of 1755 and ZY94. Colored arrows indicate open reading frames; resistance genes are marked with red triangles. Regions of >99.0% nucleotide sequence identity are shaded in gray. Black flags highlight the positions of target site duplications.